Molecular Composites from Rigid-Rod Poly(*p*-phenylene)s with Oligo(oxyethylene) Side Chains as Novel Polymer Electrolytes

U. Lauter, W. H. Meyer, and G. Wegner*

Max-Planck-Institut für Polymerforschung, Postfach 3148, D-55021 Mainz, Germany

Received July 25, 1996; Revised Manuscript Received December 20, 1996[⊗]

ABSTRACT: The preparation of new poly(*p*-phenylene)s with oligo(oxyethylene) side chains is reported. The solid state structure of the polymers as well as that of their mixtures with either lithium triflate or lithium bis(trifluoromethanesulfone)imide is described as a molecular composite consisting of rigid main chains embedded in a matrix of side-chain segments or side-chain/salt mixtures. DSC and temperature-dependent X-ray scattering prove that the side-chain matrix in the pure polymers and polymer/salt mixtures is completely amorphous. Room-temperature conductivities of more than 10^{-6} S/cm are obtained in some of these solid polymer electrolytes. Plasticization of the materials with oligo(ethyleneglycol)-dimethylether (OEGDME) improves the conductivity up to $5 \cdot 10^{-5}$ S/cm. The stiff polymer backbone induces a high mechanical plateau-modulus in the temperature range between 0 and 90 °C, which is of considerable importance for potential applications of these molecular composites as separators in rechargeable solid state lithium cells.

Introduction

For over 15 years, studies of solid polymer electrolytes (SPEs) have been actively pursued as a major contribution to the development of high-energy density batteries, particularly lithium secondary batteries.[1−3] The SPEs will act as a medium to enable lithium ion transport as well as a separator between the electrodes. Ion conductivity can be achieved using polymers that are good solvents for lithium salts and have low glass transition temperatures. With these considerations in mind, poly(ethylene oxide) is used as the basic building block for many types of linear, branched, or cross-linked SPEs. It is desired that the materials are completely amorphous even in the presence of salt.[4,5] In most studies, the target was to optimize the lithium ion conductivity alone without considering that the membranelike separator needs particular mechanical properties. Considerable improvement of the mechanical properties can be achieved by building up networks via chemical cross-linking of suitable precursor polymers[6,7] or other cross-linking methods such as γ-irradiation[8] or photo-cross-linking.[9]

Our approach for the enhancement of the mechanical strength of SPEs is the development of a material based on stiff macromolecules with short flexible oxyethylene side chains attached. These polymers belong to the class of "hairy rod molecules",[10] which have a strong tendency to self-organize into supramolecular architectures when films are cast from solution (Figure 1).[11−13] This offers the opportunity for the formation of thin films with high dimensional stability because the rigid backbones may work as reinforcing elements in an amorphous side-chain matrix. The concept of hairy rod molecules represents one way to overcome the limitations in compatibility of rigid-rod polymers and a matrix consisting of flexible compounds. These materials can thus be regarded as "molecular composites" with dispersion of both components at the molecular level.[14,15] When blended with a lithium salt, the liquidlike side-chain matrix is expected to support ion conductivity. The resulting SPE could be used as a separator in a lithium solid state cell, where the aim is to minimize the thickness of the separator membrane in order to reduce the internal resistance of the cell and maintain or even enhance the mechanical strength compared to currently used materials.

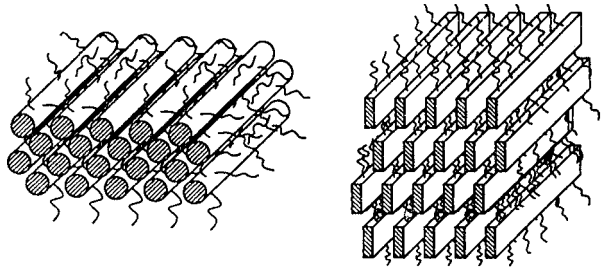

Figure 1. Schematics of molecular composites formed by chain stiff macromolecules with flexible side chains.

In this study, we report on poly(*p*-phenylene)s (PPPs) substituted with oligo(oxyethylene) side chains and blends of these novel polymers with lithium salts. In addition to their synthesis, their thermal analysis, results of X-ray scattering, mechanical properties, and ionic conductivities of the lithium salt/polymer mixtures will be described.

Results and Discussion

Monomer Synthesis. The synthetic strategy for obtaining the desired polymers is outlined in Scheme 1. The required monomeric species for an AA/BB-type Suzuki coupling,[16,17] an aromatic dibromide and an aromatic acid or ester, are prepared as follows:

Benzene-1,4-bis(boronic acid propanediol diester) (**3**) is synthesized starting from 1,4-dibromobenzene (**1**). Reaction of **1** with 2 equiv of magnesium, treatment of the resulting Grignard compound with trimethyl borate, and subsequent hydrolysis yield benzene-1,4-bis(boronic acid) (**2**), which is then esterified with 1,3-propanediol.[18]

The reaction pathway leading to 2,5-dibromo-1,4-bis(oligooxaalkyl)benzene (**8**) starts with the bromination of hydroquinone **4**.[19] Alkylation of 2,5-dibromohydroquinone (**5**) is achieved using α-(*p*-toluenesulfonyl)-ω-methoxyoligo(oxyethylene) (**7**) and potassium carbonate in DMF. High yields of **7** are obtained by tosylation of the corresponding oligo(ethyleneglycol) monomethyl ethers using tosyl chloride in the two-phase system

* To whom correspondence should be addressed.
[⊗] Abstract published in *Advance ACS Abstracts,* March 1, 1997.

S0024-9297(96)01098-4 CCC: $14.00

Scheme 1. Synthetic Route to Homopolymers PPP(EO)$_x$

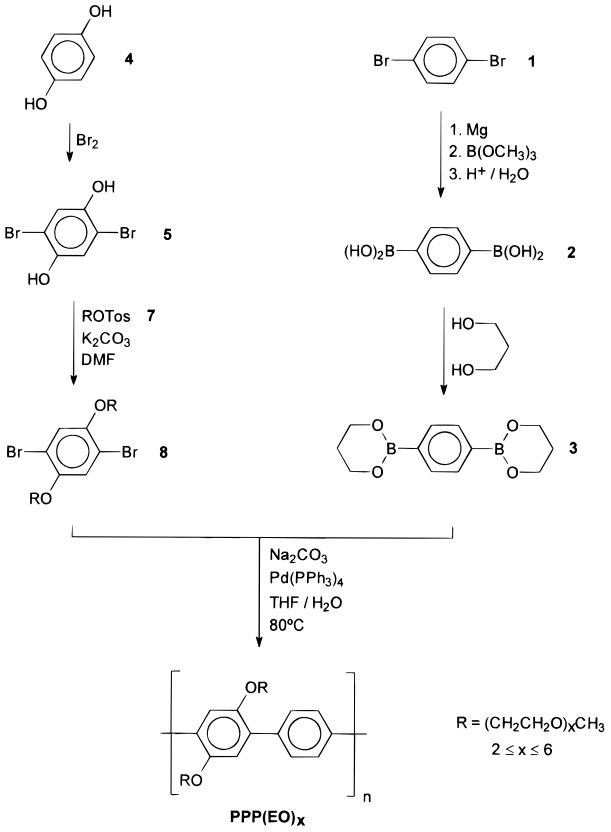

Scheme 2. Synthesis of Tetra-, Penta-, or Hexaethylene Gycol Monomethyl Ether (6) and α-(*p*-Toluenesulfonyl)-*ω*-methoxy-oligo(oxyethylene) (7)

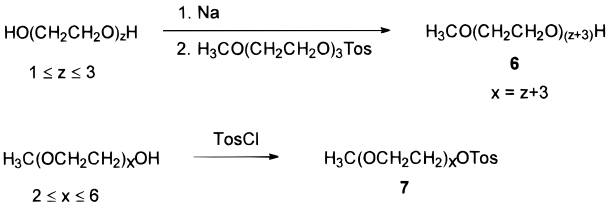

THF/aqueous NaOH at 5 °C (Scheme 2).[20] A slight excess of oligo(ethyleneglycol) monomethyl ether over tosyl chloride simplifies workup: The product can be isolated after washing with base and water; chromatographic purification is not necessary. While di- and triethylene glycol monomethyl ether are commercially available, the higher oligomers **6** were synthesized as explained in Scheme 2.

The monosodium salts of ethylene glycol, diethylene glycol, or triethylene glycol are reacted with α-(*p*-toluenesulfonyl)-*ω*-methoxytri(oxyethylene) in a Williamson-type etherification yielding tetra-, penta- or hexa(ethylene glycol) monomethyl ether, respectively. Owing to the expected ability of these "low molecular weight poly(ethylene oxide)" compounds to form crystalline complexes with low lattice energy alkali salts such as the reaction byproduct sodium tosylate,[21,22] isolation of the pure products is hampered by a complexation/decomplexation equilibrium. Therefore, fractional distillation is accompanied by successive precipitation of sodium tosylate and its oxyethylene complexes. The latter can be cleaved by treating them with acetone, which results in precipitation of sodium tosylate only; after filtration the residual solution is further distilled.

Scheme 3. Preparation of Statistical Copolymers PPP(EO)$_{x/y}$

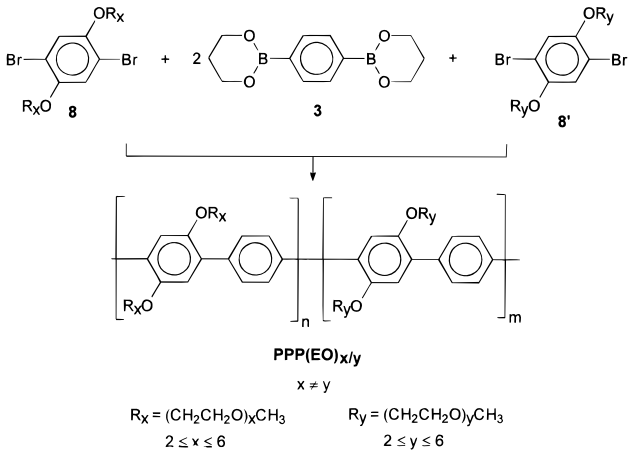

Table 1. Molecular Weight Data of PPP(EO)$_{x/y}$

Polymer	M_n[a]	M_w[a]	P_n[b]
PPP(EO)$_{2/3}$			
PPP(EO)$_{2/4}$	6100	17 600	13
PPP(EO)$_{3/4}$	6300	19 000	12
PPP(EO)$_{3/5}$	9600	31 200	17
PPP(EO)$_{4/5}$	6500	17 400	11
PPP(EO)$_{4/6}$	8000	26 700	12
PPP(EO)$_{5/6}$	8900	29 000	13

[a] GPC data calibrated by poly(*p*-phenylene) with sulfonate ester and dodecyl side chains.[23] [b] P_n calculated according to comonomer composition.

Polymer Synthesis. Synthesis of polymers PPP-(EO)$_x$ and copolymers PPP(EO)$_{x/y}$ (Schemes 1 and 3) is carried out by a Suzuki coupling reaction with Pd(0) catalysis.[23−25] Here, the indices *x* and *y* indicate the number of oxyethylene units per side chain. The polycondensation of equimolar quantities of the monomers **3** and **8** (Scheme 1) was performed in the biphasic medium THF/aqueous sodium carbonate solution at 80 °C with catalytic amounts of tetrakis(triphenylphosphine)palladium added. The polymers PPP(EO)$_x$ have a stronger tendency to crystallize, which is highly detrimental to the goal of reaching good ionic conductivity. In PPP(EO)$_3$, for example, side-chain crystallization was observed by means of DSC and X-ray diffraction.

In order to suppress the tendency to crystallize and to enhance the solubility, disorder in the side-chain matrix was created by copolymerization. Statistical copolymers PPP(EO)$_{x/y}$ were thus synthesized from 2 equiv of **3** and 1 equiv of each of the two different dibromides **8** and **8′** (Scheme 3). Therefore, copolymers PPP(EO)$_{x/y}$ have equal numbers of side chains of the length *x* and *y*. The indexes *n* and *m* in the formula of PPP(EO)$_{x/y}$ in Scheme 3 represent the fraction of the respective subunits. It is assumed that the copolymerization leads to a random copolymer, although this still needs to be proven analytically. All copolymers synthesized and their molecular weight data obtained by size exclusion chromatography (SEC) are summarized in Table 1. The SEC data were analyzed by comparison with a soluble PPP standard polymer.[26] This seems necessary, since the hydrodynamic behavior of PPP(EO)$_{x/y}$ is presumably different from common standards such as polystyrene.

All polymers show good solubility in chlorinated hydrocarbons such as chloroform. Solubility in other common organic solvents such as THF decreases with

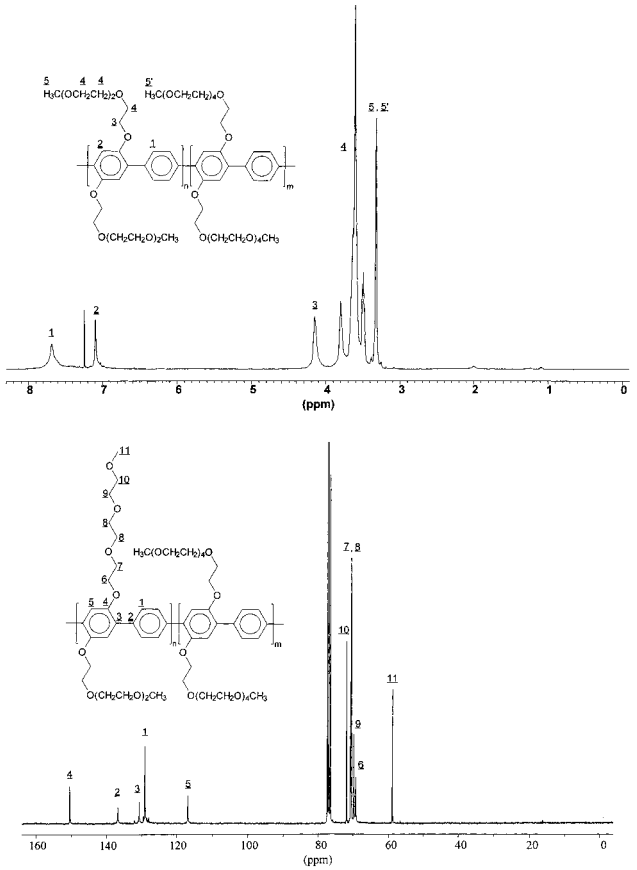

Figure 2. (a) ^{1}H NMR spectrum of PPP(EO)$_{3/5}$ in $CDCl_3$. (b) ^{13}C NMR spectrum of PPP(EO)$_{3/5}$ in $CDCl_3$.

decreasing side-chain length and increasing degree of polymerization.

The molecular structure of the polymers was assigned on the basis of their high-resolution ^{1}H and ^{13}C NMR spectra. Figure 2 shows the spectra of PPP(EO)$_{3/5}$ in $CDCl_3$ as an example. The ^{1}H NMR spectrum exhibits two rather broad singlet signals at $\delta = 7.67$ and 7.09 ppm for the two sets of aromatic protons (for a detailed data list see the Experimental Section). The two singlets at $\delta \approx 3.32$ ppm correspond to the different chemical environment of the terminate methoxy groups in the side chains. The peaks in the ^{13}C NMR spectrum can be assigned from incremental calculation[27] as well as from ^{1}H−^{13}C heteronuclear shift correlation NMR spectra.

Thermogravimetric Analysis. A first assessment of the thermal stability of the copolymers was obtained by thermogravimetry. Figure 3 shows the TGA traces for PPP(EO)$_{3/5}$ recorded under nitrogen and under oxygen. Under inert gas atmosphere, decomposition starts at ~300 °C. The weight loss arises most probably from cleavage of the bond between the phenolic oxygen and the α-methylene group. Above 450 °C, the residual material degrades further but very slowly. The weight loss points toward formation of a *p*-quinoid structure at high temperatures, but this was not studied any further. Under oxidative atmosphere, side-chain cleavage begins at 230 °C and proceeds in a two-step process. Under these conditions, even the polymer backbone decomposes in a third step at temperatures above 430 °C.

Polymer Morphology. The morphology of free-standing films cast from solutions of PPP(EO)$_{x/y}$ in chloroform was studied by X-ray diffraction with the incoming X-ray beam both parallel and perpendicular

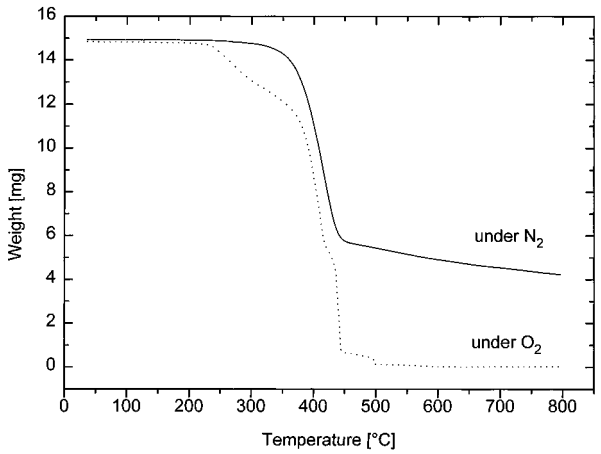

Figure 3. TGA traces of PPP(EO)$_{3/5}$ under nitrogen (straight line) and oxygen (dashed line) atmosphere.

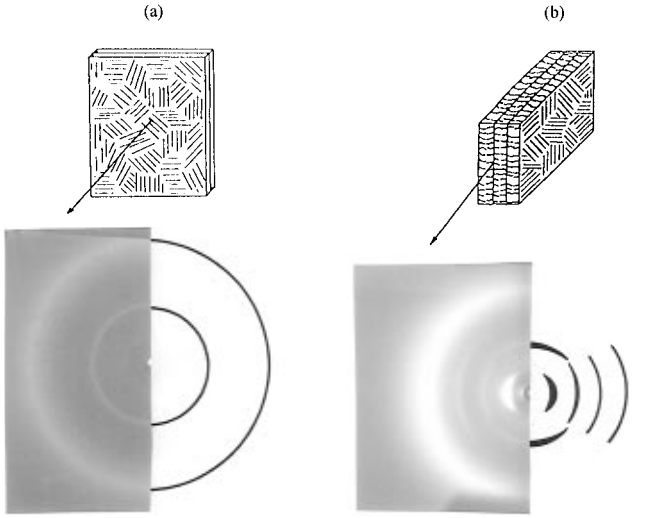

Figure 4. X-ray diffraction patterns measured for a PPP(EO)$_{3/5}$ film cast from solution with the incident beam (a) perpendicular and (b) parallel to the film surface.

to the film surface. Figure 4 shows the diffraction patterns of PPP(EO)$_{3/5}$ with the X-ray beam (a) perpendicular and (b) parallel to the film surface. In the latter, a high-intensity reflection ($n = 1$) and its higher orders ($n = 2, 3, 4$) are observed in the equatorial plane. These reflections can be assigned to a periodic lattice of layers of main chains separated by layers of side chains. The layer distance determined from the $n = 1$ reflection is $d = 19.2$ Å. The meridional reflection corresponds to the repeat unit with a d value of 8.4 Å. In Figure 4a with the X-ray beam perpendicular to the film surface, the reflection corresponding to the repeat unit appears as a circle, while the layer periodicity is hardly visible. Thus, the supramolecular structure of the film can be described as a surprisingly well ordered material consisting of layers of backbones oriented parallel to the film surface. The layers are separated by an amorphous side-chain matrix. Because the $d = 8.4$ Å reflection appears as a circle and because the layer periodicity is absent in the diffractogram with the X-ray beam perpendicular to the film surface, it can be concluded that the material forms locally ordered, but macroscopically isotropic domains within the film plane. In PPP(EO)$_{x/y}$ with longer side chains, the orientation of the layered domains parallel to the film surface decreases as the side-chain length increases. Thus, a PPP(EO)$_{5/6}$ film cast from solution consists of locally

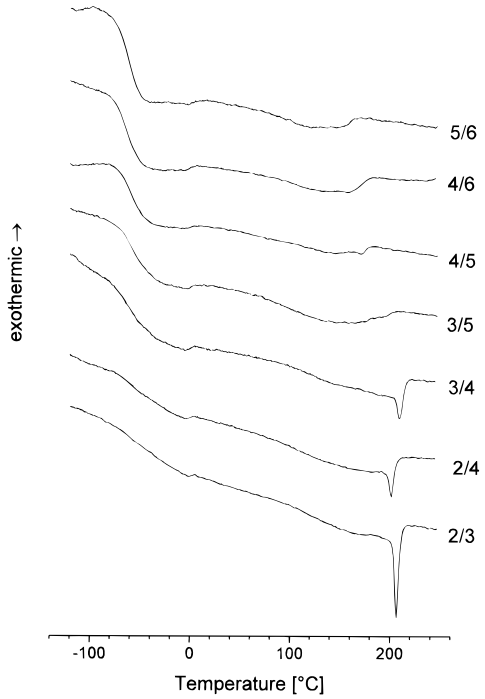

Figure 5. DSC scans of $PPP(EO)_{x/y}$ with different side-chain lengths, normalized to the same sample mass.

ordered layered domains, which are almost isotropically distributed in all three dimensions.

Phase Behavior. Investigation of the phase transitions occurring in the bulk polymers is carried out by means of DSC and X-ray scattering. Figure 5 depicts the thermograms of all $PPP(EO)_{x/y}$ samples mentioned in Table 1. In order to exclude effects from different sample history, all samples were first heated to 250 °C and then cooled to −150 °C with a scan speed of 10 K/min before measurement. Three important features are to be seen: First, at temperatures below −40 °C the side-chain glass transition occurs. With increasing number of oxyethylene segments per repeat unit, in other words with increasing side-chain length, the heat capacity change increases, while the glass transition temperatures stay relatively constant; however, the glass transition region broadens with decreasing side-chain length. The small endotherms around 0 °C probably result from very small amounts of residual water in the samples (poly(oxyethylene) is hygroscopic), although the samples had been dried carefully. Second, the thermograms do not show indications of a phase transition in the temperature range between 0 and ∼100 °C. This demonstrates that the oxyethylene side chains form an amorphous phase. Third, at higher temperatures, a broad endothermic transition is detected. In $PPP(EO)_{x/y}$ with $(x + y) \geq 8$, this event corresponds to the transition between the liquid crystalline phase of layered type and the isotropic melt, which is also confirmed by the results from polarized optical microscopy and X-ray diffraction (compare Figure 6). In $PPP(EO)_{5/6}$, for example, the melting starts at 90 °C and is complete at 160 °C. The large polydispersity of the sample presumably contributes to this behavior in a significant way.

The melting regime of $PPP(EO)_{x/y}$ shifts to higher temperatures with decreasing side-chain length, while the transition enthalpies grow (Figure 5). It seems that a fractionation takes place in the DSC experiments of $PPP(EO)_{x/y}$ with $(x + y) \leq 7$; fractions of lower molecular

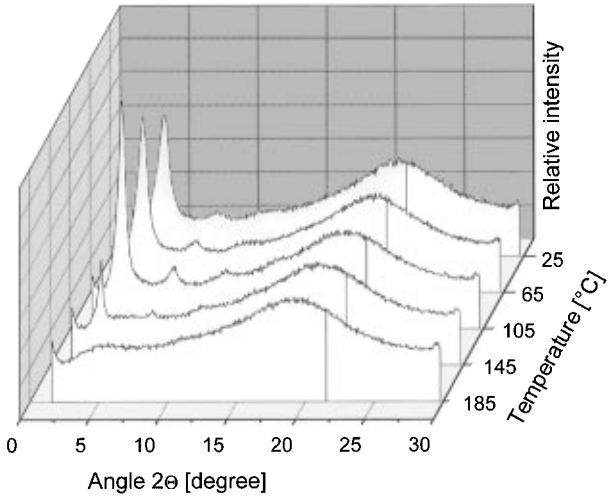

Figure 6. Temperature-dependent X-ray diffractograms of a $PPP(EO)_{5/6}$ film cast from a solution in $CHCl_3$.

weight melt into an isotropic liquid starting at temperatures around 120 °C. The sharp peaks seen in the DSC traces of $PPP(EO)_{3/4}$ (208 °C), $PPP(EO)_{2/4}$ (201 °C), and $PPP(EO)_{2/3}$ (206 °C) correspond then to the transitions of residual material of higher molecular weight into a layered liquid-crystalline phase of lower order. Behavior of this type has been recently documented in detail with samples of comparable molecular architecture by Witteler and co-workers.[28,29]

Figure 6 shows temperature-dependent X-ray reflection diffractograms of a $PPP(EO)_{5/6}$ film cast from a solution in chloroform. Similar results were obtained from all other samples with $(x + y) \geq 8$. The features seen support the interpretation of the DSC results. The diffractogram is dominated by a small-angle reflection, which has a *d* value of 22.9 Å at room temperature. This value can be attributed to the spacing between rafts of the rigid backbones, which are separated by the side-chain matrix. The first-order peak is seen very strongly and is accompanied by higher-order reflections of weaker intensity. Upon raising the temperature, the first-order reflection becomes narrower, which can be attributed to an improvement of the layered structure. The gain in intensity is due to an increase in the density difference between the raft of the backbones and the side-chain material interdigitated between the rafts. The shift to somewhat higher *d* values indicates a positive coefficient of thermal expansion. From 105 to 145 °C the intensity then decreases; at 185 °C the reflection has completely disappeared. The change in intensity most probably reflects partial melting of the fractions of lower degree of polymerization. In accordance with DSC and microscopy, an isotropic melt exists at 185 °C. Temperature-dependent X-ray scattering of $PPP(EO)_{2/4}$ (Figure 7) as an example for $PPP(EO)_{x/y}$ with $(x + y) \leq 7$ reveals the differences in phase behavior. The melting of the lower molecular weight fractions into the isotropic state causes a decreasing intensity of the small-angle reflection between 155 and 195 °C. Above 205 °C, domains of higher molecular weight form a layered liquid-crystalline phase of lower order as seen from the absence of higher-order reflections as well as from the rapid change of the layer distance (Figure 8). Evidence for the previously made statement that the oxyethylene side chains are completely amorphous is provided by the absence of any wide-angle reflections in all $PPP(EO)_{x/y}$ samples. The shape of the amorphous halo remains

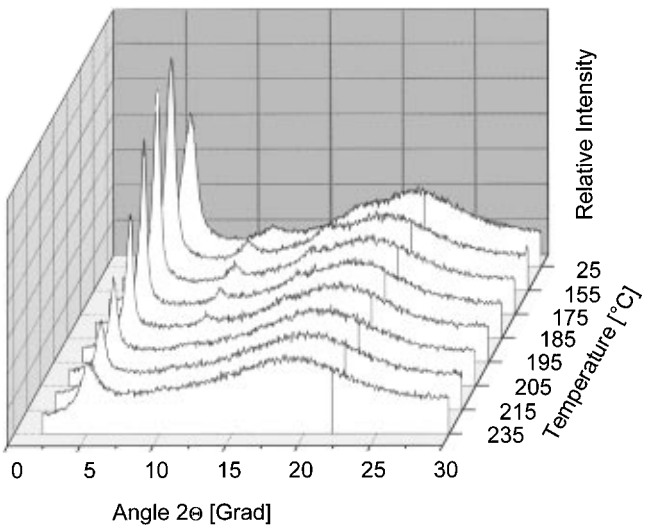

Figure 7. Temperature-dependent X-ray diffractograms of a $PPP(EO)_{2/4}$ film cast from a solution in $CHCl_3$.

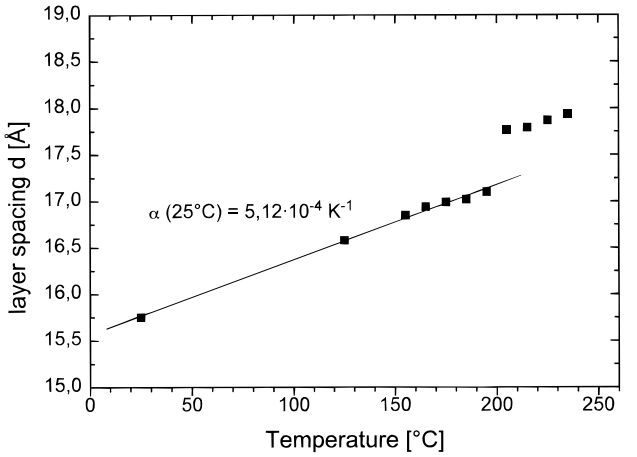

Figure 8. Layer spacings for a solution-cast film of $PPP(EO)_{2/4}$ measured at various temperatures.

unchanged over the entire temperature interval investigated.

Polymer-Salt Mixtures. All copolymers were mixed with either lithium trifluoromethanesulfonate ($LiOSO_2CF_3$, LiOTf) or lithium bis(trifluoromethanesulfone)imide ($LiN(SO_2CF_3)_2$, LiNTf) in a molar ratio of Li to O equal to 0.04, where O refers to all oxygen atoms in the side chains. DSC traces of the polymer-salt mixtures differ from those of the pure polymers by an increase of the glass transition temperature of ~25 °C (Figure 9). This effect is a likely consequence of the restriction of segmental motions due to complexation of lithium cations by oxyethylene units.[5] The T_g's of mixtures of the two salts with $PPP(EO)_{x/y}$ with $(x + y) \leq 7$ differ by ~10 °C, but since the heat capacity change observed by DSC is rather small, this observation is close to the limit of resolution. The increase in T_g of polymer-salt mixtures with longer side-chains is the same for LiOTf and LiNTf. A similar phenomenon was observed for both salt types when mixed with PEO.[30] The dependence of T_g on the total number of oxyethylene segments per repeat unit $(x + y)$ can be fitted by the equations

$$T_g = -24.057 - 5.711(x + y) + 0.197(x + y)^2 \quad \text{for } PPP(EO)_{x/y}$$

and

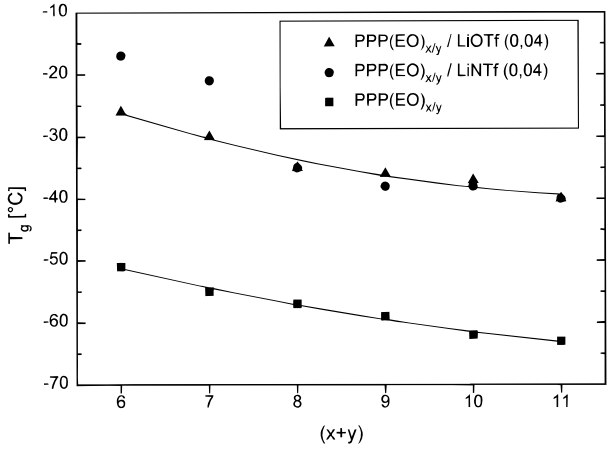

Figure 9. Influence of side-chain length $(x + y)$ and lithium salts. (concentration Li:O = 0.04) on the glass transition temperature T_g.

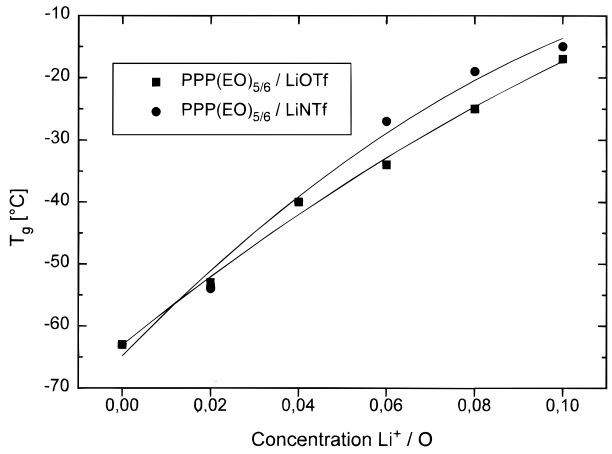

Figure 10. Concentration dependence of T_g in $PPP(EO)_{5/6}$/LiNTf and $PPP(EO)_{5/6}$/LiOTf.

$$T_g = 14.343 - 9.004(x + y) + 0.375(x + y)^2 \quad \text{for } PPP(EO)_{x/y}\text{/LiOTf}$$

The concentration dependence of T_g for $PPP(EO)_{5/6}$/lithium salt mixtures is shown in Figure 10, which illustrates the above-mentioned effect of limited segmental motion in polymer electrolytes when the salt content is increased. The T_g's for different concentrations $c_{Li:O}$ of $PPP(EO)_{5/6}$/LiOTf and $PPP(EO)_{5/6}$/LiNTf can be described respectively by the polynomials

$$T_g = -63.07 + 573.2c_{Li:O} - 1160.7(c_{Li:O})^2$$

and

$$T_g = -64.82 + 730.18c_{Li:O} - 2187.5(c_{Li:O})^2$$

It must be stressed that all of the investigated $PPP(EO)_{x/y}$/salt mixtures with a Li:O ratio of 0.04 as well as the $PPP(EO)_{5/6}$/salt mixtures in the Li:O range 0.02−0.10 are completely amorphous according to DSC and X-ray diffraction.

The d spacings observed for $PPP(EO)_{x/y}$ with and without added salt were determined from X-ray reflection of cast films at room temperature (Figure 11). Increasing the side-chain length from $(x + y) = 6$ to $(x + y) = 11$ in $PPP(EO)_{x/y}$ leads to a linear increase of the main-chain spacing from 15.8 to 22.9 Å, which can be described by the equation

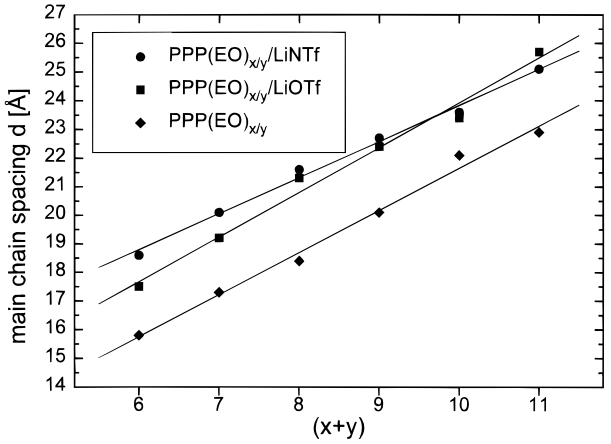

Figure 11. Main-chain spacing d in PPP(EO)$_{x/y}$, PPP(EO)$_{x/y}$/LiOTf (Li:O = 0.04), and PPP(EO)$_{x/y}$/LiNTf (Li:O = 0.04) films cast from solution.

$$d = A + B\,(x + y)$$

The slope B corresponds to an average increment of 1.47 Å/side-chain oxyethylene unit. The volume V_{EO} of one oxyethylene unit in amorphous PEO is in the range of 65 Å^3. The repeat unit of PPP(EO)$_{x/y}$ has the length of two linked phenyl groups, which is 8.4 Å as confirmed by the X-ray pattern in Figure 4a. If an orthorhombic unit cell with the cell parameters c (layer distance), b (repeat unit), and a (main chain distance within the layer) is assumed, the value of a can be estimated according to

$$a = V_{EO}/b\Delta c$$

with Δc as the measured increment of 1.47 Å/EO unit in the c direction, a sensible value of a = 5.3 Å is obtained. The ordinate intercept A = 6.9 Å corresponds to the cell parameter c in a hypothetic orthorhombic unit cell of a 2,5-dimethoxy-substituted poly(*p*-phenylene), where every second phenyl ring is substituted.

The dissolution of salt in the side-chain matrix leads to an increase of the d spacing. PPP(EO)$_{x/y}$/LiOTf mixtures (Li:O = 0.04) exhibit a linear increase in $d_{LiOTf} = A_{LiOTf} + B_{LiOTf}\,(x + y)$ with growing $(x + y)$, but with a stronger slope B_{LiOTf} = 1.56 Å in comparison to pure PPP(EO)$_{x/y}$. Since the salt content is calibrated to the oxygen content of the side chains, this behavior can be expected, if the addition of salt leads to an expansion of the assumed orthorhombic unit cell in the c axis direction only. For the PPP(EO)$_{x/y}$/LiNTf mixtures (Li:O = 0.04), one would expect an even larger slope B_{LiNTf} than B_{LiOTf} because of the larger anion size in LiNTf. This is not the case; the value of B_{LiNTf} is 1.25 Å. The reason for this behavior is presently unclear. One possible interpretation could be that the addition of LiNTf to PPP(EO)$_{x/y}$ leads to a two-dimensional "swelling" in the direction of the layer distance c and the main-chain distance b within the layer.

Ion Conductivities. Figure 12a shows the temperature-dependent dc conductivities of PPP(EO)$_{x/y}$/LiOTf for a constant molar ratio of Li:O = 0.04, as obtained from impedance spectroscopy using two blocking gold electrodes. The conductivity σ as a function of the inverse temperature can be fitted by the Williams−Landel−Ferry (WLF) equation[31,32]

$$\sigma(T) = \sigma_0 \exp\left[\frac{C_1(T - T_g)}{(C_2 + T - T_g)}\right]$$

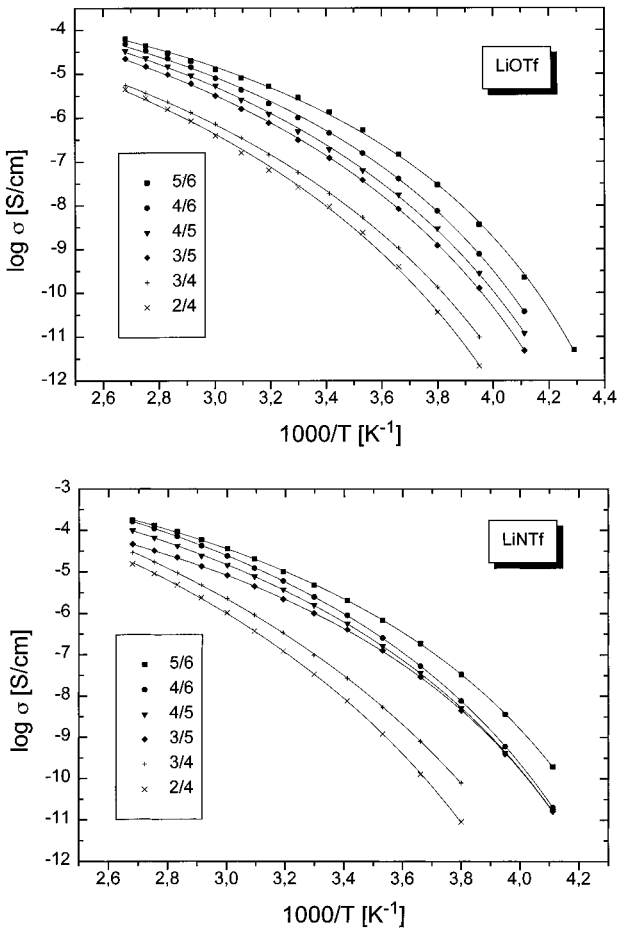

Figure 12. Ion conductivities vs T^{-1} at constant salt concentration Li:O = 0.04, (a) PPP(EO)$_{x/y}$/LiOTf; (b) PPP(EO)$_{x/y}$/LiNTf.

Table 2. WLF Parameters for PPP(EO)$_{x/y}$/LiOTf (Li:O = 0.04)

x/y	C_1	C_2 (K)	T_g (K)	log σ_0 (S/cm)
2/4	25.31	66.53	247	−12.58
3/4	24.75	62.19	243	−12.51
3/5	24.46	55.47	238	−12.21
4/5	23.97	54.43	237	−11.96
4/6	22.72	48.28	236	−11.70
5/6	21.54	43.12	233	−11.37

where T_g is the glass transition temperature (taken from DSC measurements), σ_0 is the conductivity at $T = T_g$ and C_1 and C_2 are constants. The lines in Figure 12 are the results of fitting at temperatures above T_g (all parameters allowed to vary except T_g). A compilation of the WLF fitting parameters for PPP(EO)$_{x/y}$/LiOTf (Li:O = 0.04) is given in Table 2.

Figure 12a demonstrates that extending the average side-chain length $^1/_2(x + y)$ from 3 to 5.5 oxyethylene units enhances the room-temperature conductivity by more than two decades from 10^{-8} (PPP(EO)$_{2/4}$) to 1.4 × 10^{-6} S/cm (PPP(EO)$_{5/6}$). These values agree well with literature data for similar polymer electrolytes that consist of a stiff helical polyglutamate main chain with oxyethylene side chains.[33] It should be recalled that the rather high conductivity in these systems is promoted by short oxyethylene chains, one end of which is immobile due to the covalent bond to the rigid rod backbone. The change from LiOTf to LiNTf as a provider of charge carriers (Figure 12b) leads to an improvement of conductivity, especially at high temperature. At 100 °C, PPP(EO)$_{5/6}$/LiNTf has a conductivity of better than 10^{-4} S/cm. The conductivity enhance-

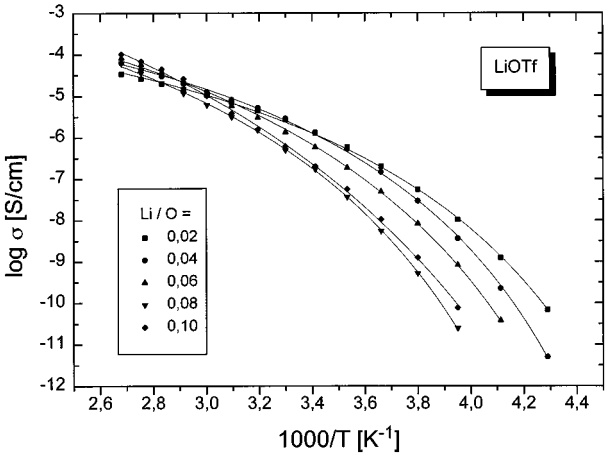

Figure 13. Temperature dependence of ionic conductivity for $PPP(EO)_{5/6}$/LiOTf complexes at various LiOTf concentrations.

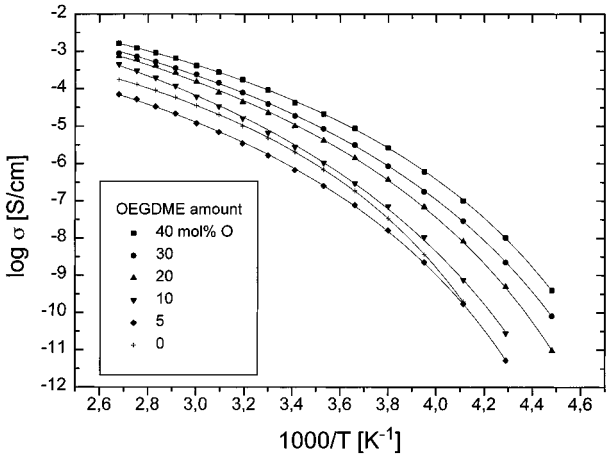

Figure 14. Influence of the amount of plasticizer OEGDME on the conductivity of $PPP(EO)_{5/6}$/LiNTf.

ment by LiNTf as compared to LiOTf is commonly attributed to the plasticizing effect of the large and highly polarizable anion NTf^- in complexes with PEO.[34]

The concentration and temperature dependence of the conductivity of $PPP(EO)_{5/6}$/LiOTf is shown in Figure 13. These results are understood in terms of the simple relation for the ion conductivity

$$\sigma(T) = n(T)\mu(T)e$$

where n is the number of charge carriers, μ their mobility, and e the unit electric charge. At low temperatures, the influence of the side-chain matrix glass transition is reflected. At −10 °C, the salt-rich polymer electrolytes are only slightly above T_g. Ionic conductivity is hampered owing to slow segmental motion, which gives rise to a small value of μ. At the same temperature, however, the mixture with a salt content of Li:O equal to 0.02 is already more than 40 °C above T_g. As a consequence, the conductivity has a value more than two decades higher. At 100 °C on the other hand, conductivity is mainly given by the total number of charge carriers n, so that the electrolyte with Li:O equal to 0.10 becomes the best lithium ion conductor.

Further improvement of the ionic conductivity was attained by plasticizing the solid polymer electrolytes with oligo(ethylene glycol) dimethyl ether (OEGDME) of an average molecular weight of 550, corresponding to an average degree of polymerization of 11.5 oxyethylene units. $PPP(EO)_{5/6}$ was mixed with OEGDME and LiNTf to give polymer electrolytes with different OEGDME content but constant Li:O concentration of 0.04, counting the OEGDME as part of the polymer matrix (Figure 14). Surprisingly, addition of 5 mol % OEGDME to the sample leads to a decrease in conductivity compared to the unplasticized SPE. This behavior may be explained by an antiplasticizing effect, which means that small amounts of plasticizer would occupy a part of the free volume in the polymer electrolyte. Any decrease in free volume would cause a drop in ionic mobility. Upon addition of larger amounts of OEGDME, however, the expected influence of the plasticizer on the segmental motion of the entire side-chain matrix enhances the ionic conductivity. Thus, samples with more than 10 mol % OEGDME exhibit better lithium ion conductivity compared to the unplasticized $PPP(EO)_{5/6}$/LiNTf; σ reaches values of 4.3×10^{-5} S/cm at room temperature in the case of an OEGDME content equal to 40 mol % O. This value is in the range typically found for completely amorphous PEO/LiNTf SPEs.[35]

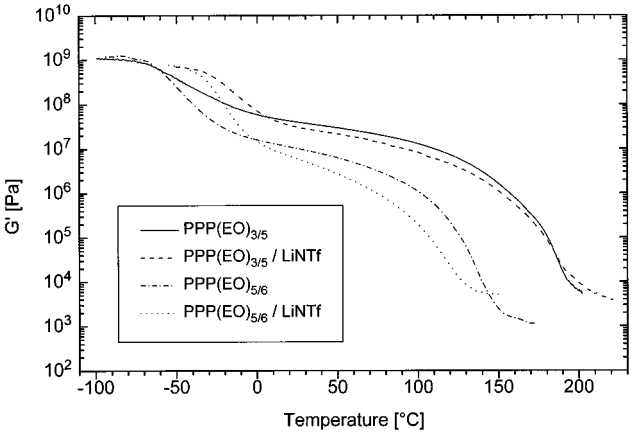

Figure 15. Temperature dependence of shear storage modulus G' for melt-pressed pellets of $PPP(EO)_{3/5}$, $PPP(EO)_{5/6}$, and their mixtures with LiNTf (Li:O = 0.04).

Dynamic Mechanical Properties. In order to prove the accuracy of our concept of preparing a molecular composite material with improved mechanical strength, its viscoelastic behavior was analyzed. Figure 15 shows the temperature dependence of the storage moduli G' of two polymers with long ($PPP(EO)_{5/6}$) and medium ($PPP(EO)_{3/5}$) side-chain length, as well as G' of two mixtures with LiNTf of the same polymers. The following characterisitic features are seen: Starting from a value of 10^9 Pa in the glassy state of $PPP(EO)_{3/5}$, the modulus decreases by 1−2 orders of magnitude as the oxyethylene side chain undergoes its glass transition between −80 and ∼−10 °C. In the technically important temperature range from about 0 to 100 °C, however, the modulus stays rather constant at a considerably high plateau value between 5×10^7 and 10^7 Pa; this clearly demonstrates the reinforcing effect of the stiff main chains on the liquidlike side-chain matrix. Between 100 and 200 °C, the broad main-chain melting process gives rise to a strong decrease of G', and typical values of a viscous melt are reached. In general, the corresponding SPE composed of $PPP(EO)_{3/5}$/LiNTf exhibits the same behavior except that the glass transition occurs at higher temperatures in agreement with DSC results. As expected, the drop in modulus of $PPP(EO)_{5/6}$ at T_g is larger owing to the higher oxyethylene content of the material. For the same reason, the rubbery plateau ends with the onset of main-chain melting at ∼90 °C. In the $PPP(EO)_{5/6}$/LiNTf system, the plateau extends over a smaller temperature range, since the

volume fraction of main chains is smaller and, thus, their reinforcing effect is not as strong as in the former case.

Conclusions. New polymers based on a poly(*p*-phenylene) backbone with oligo(oxyethylene) side chains attached have been prepared with emphasis on tuning of the side-chain length in order to optimize the solid state behavior. The supramolecular structure of the polymers $PPP(EO)_{x/y}$ was shown to consist of stiff main-chain layers embedded in an amorphous matrix of the side-chain segments. A molecular composite is thus formed which undergoes melting above 90 °C; the exact value of the melting temperature depends on the length of the backbone and side chains. $PPP(EO)_{x/y}$ with longer ($(x + y) \geq 8$) side chains form an isotropic melt. The molten state of polymers with short side chains contains both isotropic and anisotropic components.

The reinforcing effect of the main chains on the liquidlike oxyethylene matrix, either with or without lithium salt added, leads to a large improvement in the mechanical properties in comparison to pure amorphous PEO derivatives or SPEs prepared from them. Although only the side-chain phase of such molecular composites contributes to conductivity, relatively high ion conductivities of more than 10^{-6} S/cm at ambient temperature are obtained in mixtures with lithium salts. The conductivity behavior of these materials is rather close to that of polymer electrolytes prepared from amorphous PEO, but the mechanical properties are considerably improved. The temperature dependence of the conductivity is described by a WLF-fitting procedure indicating that charge carrier mobility is controlled by the free volume of the sample. Addition of oligo(ethyleneglycol)dimethyl ether as a plasticizer raises the conductivity by 1.5 orders of magnitude (to 5×10^{-5} S/cm), with some loss of mechanical strength.

Experimental Section

Measurements. ^{1}H and ^{13}C NMR data were obtained with a Bruker AC 300 (300 MHz) spectrometer using $CDCl_3$ as chemical shift standard. UV/visible spectra were recorded on a Perkin-Elmer Lambda 3 spectrophotometer and FT-IR spectra on a Perkin-Elmer Paragon 1000 spectrometer. Mass spectra were obtained from a VG-Biotech Trio-2000 instrument with EI ionization (70 eV). The morphology of solution-cast films was characterized by X-ray diffraction using a flat-film camera with Ni-filtered Cu Kα radiation. Wide-angle X-ray scattering was performed on a Philips PW 1820 powder diffractometer (room temperature) and a Siemens D 500 diffractometer (elevated temperature). Thermogravimetry was done on a Mettler TG 50 with a heating rate of 10 K/min. DSC measurements were carried out under nitrogen with a heating rate of 10 K/min on a Mettler DSC TA 3000 instrument; glass transition temperatures (T_g's) were taken as the midpoints of the Δc_p step. Ion conductivities of polymer electrolytes were determined using a Schlumberger SI 1260 impedance/gain phase analyzer with a homemade dielectric interface in the frequency range from 10^{-1} to 10^5 Hz. The measurements were performed in a Novocontrol cryostat. The sample temperature was regulated by a temperature-controlled nitrogen gas jet and measured with a platinum resistor (Pt 100) inserted in one electrode. For SPE sample preparation, polymer/salt mixtures were dissolved in 1,2-dichloroethane. If the dissolution of salt was incomplete, a few drops of methanol were added to fully dissolve the polymer electrolyte. For conductivity measurements, the solution was cast onto gold electrodes. After evaporation of the solvent, the films were vacuum dried at 70−80 °C for at least 24 h. In order to provide good electrode contact, the gold counterelectrode was vaporized on the polymer electrolyte film. dc conductivities were obtained from Cole−Cole plots (Z'' vs Z') and were identical with the low-frequency plateau of the ac conductivities. The viscoelastic properties of melt-pressed pellets were measured with a Rheometrics RMS-800 instrument at a cooling rate of 2 K/min and a frequency of 10 rad/s.

Materials. All reagents and solvents were purchased from Merck, Fluka, or Aldrich and were used without further purification unless otherwise stated. In order to remove peroxide impurities and oxygen, THF for polymerization reactions was refluxed with sodium and distilled under argon. Water for the polymerization procedure was deliberated from dissolved oxygen by bubbling a nitrogen stream through for 3 hs at 60−70 °C. Benzene-1,4-bis(boronic acid)propanediol diester[15] and 2,5-dibromohydroquinone[16] were prepared as described. $LiOSO_2CF_3$ from Aldrich and $LiN(SO_2CF_3)_2$ from 3M were used for the preparation of polymer electrolytes; both were dried in vacuo at 150 °C before use.

General Procedure for Synthesis of Oligo(ethyleneglycol) Monomethyl Ether (α-Hydro-ω-methoxyoligo(oxyethylene)) (6). Glycol (2.4 mol; 149 g of ethyleneglycol, 254 g of diethylene glycol, or 360 g of triethylene glycol) is stirred under dry nitrogen at 100 °C while 0.68 mol (15.64 g) of sodium in small portions is carefully added. After all the sodium has reacted, the flask content is cooled to 50 °C and 0.6 mol (191.1 g) of α-(*p*-toluenesulfonyl)-ω-methoxytris(oxyethylene) is added dropwise over 1 h. A white precipitate of sodium tosylate appears after a few minutes. Stirring is continued at 100 °C for 24 h, after which the solution is cooled to room temperature and filtered. The filter remainder is washed with acetone. After evaporation of the solvent acetone, the resulting liquid is fractionated in vacuum. The first fraction contains excess glycol, the second fraction the product. Filtration of the distillation remainder, washing of the filter cake with acetone, and repeating of the distillation procedure gives an additional amount of product.

(a) Tetraethylene Glycol Monomethyl Ether (α-Hydro-ω-methoxytetrakis(oxyethylene)): yield 77.48 g (63%) of a colorless oil; (bp (0.05 mbar) 105−108 °C; ^{1}H NMR ($CDCl_3$) δ 3.78−3.41 (m, 16H, OCH_2), 3.30 (s, 3H, OCH_3), ∼2.8 (s, 1H, OH) ppm; ^{13}C NMR ($CDCl_3$) δ 72.3 (CH_2CH_2OH), 71.7 (CH_2-OCH_3), 70.3, 70.2, 70.1 (OCH_2CH_2O), 61.4 (CH_2OH), 58.7 (OCH_3) ppm.

(b) Pentaethylene Glycol Monomethyl Ether (α-Hydro-ω-methoxypentakis(oxyethylene)): yield 116.71 g (77%) of a colorless oil; bp (0.05 mbar) 124−126 °C; ^{1}H NMR ($CDCl_3$) δ 3.77−3.41 (m, 20H, OCH_2), 3.30 (s, 3H, OCH_3), ∼2.8 (s, 1H, OH) ppm; ^{13}C NMR ($CDCl_3$) δ 72.5 (CH_2CH_2OH), 71.9 (CH_2-OCH_3), 70.5, 70.4, 70.3 (OCH_2CH_2O), 61.6 (CH_2OH), 58.9 (OCH_3) ppm.

(c) Hexaethylene Glycol Monomethyl Ether (α-Hydro-ω-methoxyhexakis(oxyethylene)) yield 101.36 g (57%) of a colorless oil; bp (0.05 mbar) 150−154 °C; ^{1}H NMR ($CDCl_3$) δ 3.74−3.42 (m, 24H, OCH_2), 3.30 (s, 3H, OCH_3), ∼2.9 (s, 1H, OH) ppm; ^{13}C NMR ($CDCl_3$) δ 72.6 (CH_2CH_2OH), 71.9 (CH_2-OCH_3), 70.6, 70.4 (OCH_2CH_2O), 61.6 (CH_2OH), 59.0 (OCH_3) ppm.

General Procedure for Synthesis of α-(*p*-Toluenesulfonyl)-ω-methoxyoligo(oxyethylene) (7). The solution of 0.285 mol (11.4 g) of sodium hydroxide in 60 mL of water (5 M NaOH) is added to a solution of 0.2 mol of oligo(ethylene glycol) monomethyl ether in 50 mL of THF. The mixture is cooled below 5 °C. Stirring vigorously and maintaining the reaction mixture at that temperature, a solution of 0.19 mol (36.2 g) of *p*-toluenesulfonyl chloride in 50 mL of THF is added dropwise. Stirring is continued for 2 h more. The mixture is placed in a separation funnel, and the phases are separated. The aqueous phase is extracted with diethyl ether (3 × 50 mL). The organic phases are combined and washed with water until the washing water has a pH value of 7. After drying over sodium sulfate, the solvent is evaporated yielding a clean pale yellowish oil.

α-(*p*-Toluenesulfonyl)-ω-methoxytris(oxyethylene): Yield 54.45 g (90%); ^{1}H NMR ($CDCl_3$) δ 7.77 (d, $J = 8$ Hz, 2H, RO_3-$SC(CH)_2$), 7.31 (d, $J = 8$ Hz, 2H, $H_3CC(CH)_2$), 4.13 (t, 2H, SO_3-CH_2), 3.65 (t, 2H, $SO_3CH_2CH_2$), 3.62−3.45 (m, 8H, OCH_2), 3.34 (s, 3H, OCH_3), 2.41 (s, 3H, $ArCH_3$) ppm; ^{13}C NMR ($CDCl_3$) δ 144.7 ($ArCCH_3$), 133.2 ($ArCSO_3R$), 129.7 ($Ar(CH)_2CCH_3$), 127.9

($Ar(CH)_2CSO_3R$), 71.9 (CH_2OCH_3), 70.7, 70.5 (OCH_2CH_2O), 69.2 ($ArSO_3CH_2CH_2O$), 68.6 ($ArSO_3CH_2CH_2O$), 58.9 (OCH_3), 21.5 ($ArCH_3$) ppm; IR (film) ν 3047 (vw, ν_{C-H}, Ar—H), 2878 (s, ν_{C-H}, CH_2, CH_3), 1598 (m, $\nu_{C=C}$, Ar—C═C), 1495 (w, $\nu_{C=C}$, Ar—C═C), 1453 (m, δ_{C-H}, CH_2), 1357 (vs, $\nu_{S=O}$, SO_2O), 1077 (vs, SO_2O), 1098 (vs, ν_{C-O}, $ROCH_2$), 818 (m, $\nu\delta_{C-H}$, Ar—C—H) cm^{-1}; MS (EI) m/z 319 (M^+, 4), 274 ($M^+ - CH_2OCH_3$, 3), 243 ($M^+ - OCH_2CH_2OCH_3$, 9), 199 ($M^+ - O(CH_2CH_2O)_2CH_3$, 100), 155 ($ArSO_2^+$, 69), 103 ($(CH_2CH_2O)_2CH_3^+$, 19), 91 (Ar^+, 98), 59 ($CH_2CH_2OCH_3^+$, 84).

Equivalent data are available for the following products: α-(*p*-toluenesulfonyl)-*ω*-methoxybis(oxyethylene), yield 91%; α-(*p*-toluenesulfonyl)-*ω*-methoxytetrakis(oxyethylene), yield 85%; α-(*p*-toluenesulfonyl)-*ω*-methoxypentakis(oxyethylene), yield 86%; α-(*p*-toluenesulfonyl)-*ω*-methoxyhexakis(oxyethylene), yield 80%.

General Procedure for Synthesis of 2,5-Dibromo-1,4-bis(oligooxaalkyl)benzene (8). A suspension of 0.148 mol of α-(*p*-toluenesulfonyl)-*ω*-methoxyoligo(oxyethylene), 0.075 mol (20.10 g) of 2,5-dibromohydroquinone, and 0.225 mol (31.1 g) of potassium carbonate in 180 mL of DMF is heated to 80 °C for 5 h and stirred for an additional 12 h at room temperature.

(a) Workup for Compounds with Short Side Chains (no More Than Four Oxyethylene Units). The reaction mixture is filtered, and the filter remainder is washed with 100 mL of diethyl ether. Upon addition of 300 mL of water, the phases are separated and the aqueous phase is extracted with diethyl ether. The combined organic phases are first extracted with small amounts of diluted sodium hydroxide solution in order to remove unreacted phenolic compounds. Then the organic phase is washed several times with small amounts of water. After drying over sodium sulfate, the solvent is evaporated. The product is usually obtained in high purity and can be recrystallized from ethanol at −20 °C if necessary.

(b) Workup for Compounds with Long Side Chains (Five or Six Oxyethylene Units). The reaction mixture is diluted with 200 mL of water and subjected to a continuous extraction with diethyl ether in a perforator for 36 h. The organic phase is transferred to a separation funnel and washed several times with small amounts of saturated sodium chloride solution. After drying over sodium sulfate and evaporation of the solvent, a yellowish oil is obtained. Purification is performed by column filtration using silica gel and dichloromethane/methanol (10:1, v/v) as eluent.

2,5-Dibromo-1,4-bis(1,4,7,10-tetraoxaundecanyl)benzene: yield 88% of a viscous liquid, that crystallizes slowly (mp 33−34 °C); ^{1}H NMR ($CDCl_3$) δ 7.13 (s, 2H, ArH), 4.10 (t, 4H, $ArOCH_2$), 3.84 (t, 4H, $ArOCH_2CH_2$), 3.75 (t, 4H, $ArOCH_2CH_2OCH_2$), 3.70−3.59 (m, 8H, OCH_2), 3.52 (t, 4H, H_3COCH_2), 3.36 (s, 6H, OCH_3) ppm; ^{13}C NMR ($CDCl_3$) δ 150.3 (ArCOR), 119.2 (ArCH), 111.3 (ArCBr), 71.9 (CH_2OCH_3), 71.0 (OCH_2CH_2O), 70.6, 70.5, 70.1 ($ArOCH_2CH_2$), 69.5 ($ArOCH_2$), 58.9 (OCH_3) ppm; IR (film) ν 3081 (vw, ν_{C-H}, Ar—H), 2873 (vs, ν_{C-H}, CH_2, CH_3), 1492 (s, $\nu_{C=C}$, Ar—C═C), 1451 (m, ν_{C-H}, CH_2), 1109 (vs, ν_{C-O}, RO—CH_2), 853 (m, ν_{CH_2}, CH_2), 781 (w, ν_{C-Br}, C—Br) cm^{-1}; MS (EI) m/z = 560 (M^+, 9), 147 ($(CH_2CH_2O)_3CH_3^+$, 83), 103 ($(CH_2CH_2O)_2CH_3^+$, 92), 59 ($CH_2CH_2OCH_3^+$, 100).

Analogous data are obtained from the following compounds: 2,5-Dibromo-1,4-bis(1,4,7-trisoxaoctyl)benzene, yield 90%, mp 52 °C; 2,5-Dibromo-1,4-bis(1,4,7,10,13-pentaoxatetradecanyl)benzene, yield 84%, mp 43−44 °C; 2,5-dibromo-1,4-bis(1,4,7,10,13,16-hexaoxaheptadecanyl)benzene, yield 79%; 2,5-dibromo-1,4-bis(1,4,7,10,1316,19-heptaoxaeicosanyl)benzene, yield 84%.

Synthesis of Polymers PPP(EO)$_{x/y}$. 2,5-Dibromo-1,4-bis(oligooxaalkyl)benzene (0.024 mol), 0.024 mol (5.90 g) of benzene-1,4-bis(boronic acid)propane-1,3-diol diester, and 0.28 mol (29.68 g) of sodium carbonate are set under argon atmosphere. An 280 mL aliquot of absolute THF, 0.36 mmol (0.416 g, 1.5 mol %) of tetrakis(triphenylphosphine)palladium, and 280 mL of water are added, and the resulting solution is vigorously stirred for 72 h under reflux. Since the palladium catalyst is oxygen and light sensitive, care must be taken to exclude oxygen from the reaction mixture and to protect the reaction vessel from sunlight.

Workup for Polymers with Short Side Chains ($(x + y) \leq 8$). After cooling to room temperature, the mixture is poured into a 5-fold excess (v/v) of methanol. The precipitate is filtered off, taken up in dichloromethane, and filtrated again. The volume of the resulting solution is reduced, and the polymer is reprecipitated from methanol. Depending on the degree of purity, the product is obtained as a pale yellow or brownish solid. Further purification may be performed by silica gel filtration using first dichloromethane and then dichloromethane/methanol (∼50:1, v/v) as eluent. Yield >90%.

(b) Workup for Polymers with Long Side Chains ($(x + y) \geq 9$). After cooling to room temperature, the phases are separated. The (still water containing) THF phase is poured into a 5-fold excess (v/v) of petrol ether. The gelatinous precipitate is filtered off, taken up in dichloromethane, and filtered again. The resulting polymer solution is evaporated to dryness and reprecipitated from petroleum ether. In order to remove traces of sodium carbonate, the crude polymer is extracted with water in a Soxhlet apparatus, until the washing water is no longer alkaline. Depending on the degree of purity, the product is obtained as a pale yellow or brownish solid. Further purification may be performed by silica gel filtration using first dichloromethane and then dichloromethane/methanol (∼50:1, v/v) as eluent. Yield >82%.

$PPP(EO)_{3/5}$: ^{1}H NMR ($CDCl_3$) δ 7.67 (s, 4H, *1*), 7.09 (s, 2H, 2), 4.15 (m, 4H, 3), 3.95−3.42 (m, 28H, 4), 3.320 (s, 3H, 5), 3.318 (s, 3H, **5′**) ppm; ^{13}C NMR ($CDCl_3$) δ 150.5 (4), 136.8 (2), 130.7 (3), 129.1 (**1**), 116.8 (5), 71.9 (10), 70.8 (9), 70.7−70.4 (8), 69.8 (7), 69.3 (6), 58.9 (11) ppm; IR (solution-cast film) ν 2872 (s, ν_{C-H}, CH_2, CH_3), 1487 (s, $\nu_{C=C}$, Ar—C═C), 1455 (m, δ_{C-H}, CH_2), 1108 (vs, ν_{C-O}, RO—CH_2), 844 (m, ν_{CH2}, CH_2) cm^{-1}; UV/Vis ($CHCl_3$) λ 349, 290 nm. Anal. Calcd for $(C_{30}H_{44}O_{10})_n$: C, 63.81; H, 7.85; O, 28.33. Found: C, 63.00; H, 7.90; O, not determined.

$PPP(EO)_{2/3}$. Anal. Calcd for $(C_{24}H_{32}O_7)_n$: C, 66.65; H, 7.46; O, 25.89. Found: C, 66.13; H, 7.52; O, not determined.

$PPP(EO)_{2/4}$. Anal. Calcd for $(C_{26}H_{36}O_8)_n$: C, 65.53; H, 7.61; O, 26.86. Found: C, 64.43; H, 7.55; O, not determined.

$PPP(EO)_{3/4}$. Anal. Calcd for $(C_{28}H_{40}O_9)_n$: C, 64.60; H, 7.74; O, 27.66. Found: C, 63.65; H, 7.83; O, not determined.

$PPP(EO)_{3/6}$. Anal. Calcd for $(C_{32}H_{48}O_{11})_n$: C, 63.14; H, 7.95; O, 28.91. Found: C, 60.09; H, 8.03; O, not determined.

$PPP(EO)_{4/5}$. Anal. Calcd for $(C_{32}H_{48}O_{11})_n$: C, 63.14; H, 7.95; O, 28.91. Found: C, 62.02; H, 8.09; O, not determined.

$PPP(EO)_{4/6}$. Anal. Calcd for $(C_{34}H_{52}O_{12})_n$: C, 62.56; H, 8.03; O, 29.41. Found: C, 61.98; H, 8.05; O, not determined.

$PPP(EO)_{5/6}$. Anal. Calcd for $(C_{36}H_{56}O_{13})_n$: C, 62.05; H, 8.10; O, 29.85. Found: C, 61.45; H, 7.99; O, not determined.

^{1}H and ^{13}C NMR spectra of all derivatives $PPP(EO)_{x/y}$ are analogous to those of $PPP(EO)_{3/5}$ and show the expected signals for the respective side-chain pattern.

Acknowledgment. Financial support from BMBF (Förderkennzeichen 03N3007B9) is gratefully acknowledged. We also thank Dr. S. Höger, Dr. V. Enkelmann, Dr. G. Lieser, and Dr. T. Pakula for valuable discussions and Professor B. M. Foxman (Brandeis University, Waltham, MA) for help with the English in this article.

References and Notes

(1) Armand, M.; Sanchez, J. Y.; Gauthier, M.; Choquette, Y. In *Electrochemistry of Novel Materials*; Lipkowski, J., Ross, P. N., Eds.; VCH Publishers: New York, 1994.
(2) Gauthier, M.; Belanger, A.; Kapfer, B.; Vassort, G.; Armand, M. In *Polymer Electrolyte Reviews*; MacCallum, J. R., Vincent, C. A., Eds.; Elsevier Applied Science: London, 1989; Vol. 2.
(3) Abraham, K. M. *Electrochim. Acta* **1993**, *38*, 1233.
(4) Takeoka, S.; Ohno, H.; Tsuchida, E. *Polym. Adv. Technol.* **1993**, *4*, 53.
(5) Armand, M. *Solid State Ionics* **1994**, *69*, 309.
(6) Le Nest, J. F.; Gandini, A.; Cheradame, H. *Br. Polym. J.* **1988**, *20*, 253.
(7) Le Nest, J. F.; Gandini, A.; Xu, L.; Schoenenberger, C. *Polym. Adv. Technol.* **1993**, *4*, 92.

(8) Nazri, G. A.; Meibuhr, S. G. *J. Electrochem. Soc.* **1989**, *136*, 2450.
(9) Tada, Y.; Sato, M.; Takeno, N.; Kameshima, T.; Nakacho, Y.; Shigehara, K. *Macromol. Chem. Phys.* **1994**, *195*, 571.
(10) Ballauff, M. *Angew. Chem., Int. Ed. Engl.* **1989**, *28*, 253.
(11) Wegner, G. *Thin Solid Films* **1992**, *216*, 105.
(12) Wegner, G. *Mol. Cryst. Liq. Cryst.* **1993**, *235*, 1.
(13) Helmer-Metzmann, F.; Ballauff, M.; Schulz, R. C.; Wegner, G. *Makromol. Chem.* **1989**, *190*, 985.
(14) Krause, S. J.; Haddock, T. B.; Price, G. E.; Adams, W. W. *Polymer* **1988**, *29*, 195.
(15) Ciferri, A. *Polym. Eng. Sci.* **1994**, *34*, 377.
(16) Miyaura, N.; Yanagi, T.; Suzuki, A. *Synth. Commun.* **1981**, *11*, 513.
(17) Schlüter, A.-D.; Wegner, G. *Acta Polym.* **1993**, *44*, 59.
(18) Coutts, I. G. C.; Goldschmid, H. R.; Musgrave, O. C. *J. Chem. Soc.* **1970**, *488*.
(19) Tietze, L. F.; Eicher, T. *Reaktionen und Synthesen im organisch-chemischen Praktikum und Forschungslaboratorium*; Georg Thieme Verlag: Stuttgart, 1991, p 274.
(20) Ouchi, M.; Inoue, Y.; Liu, Y.; Nagamune, S.; Nakamura, S.; Wada, K.; Hakushi, T. *Bull. Chem. Soc. Jpn.* **1990**, *63*, 1260.
(21) Wright, P. V. *Br. Polym. J.* **1975**, *7*, 319.
(22) Wright, P. V. In *Polymer Electrolyte Reviews*; MacCallum, J. R., Vincent, C. A., Eds.; Elsevier Applied Science: London, 1989; Vol. 2.
(23) Rehahn, M.; Schlüter, A.-D.; Wegner, G.; Feast, W. J. *Polymer* **1989**, *30*, 1060.
(24) Vahlenkamp, T.; Wegner, G. *Macromol. Chem. Phys.* **1994**, *195*, 1933.
(25) Remmers, M.; Schulze, M.; Wegner, G. *Macromol. Rapid Commun.* **1996**, *17*, 239.
(26) Vanhee, S.; Rulkens, R.; Lehmann, U.; Rosenauer, C.; Schulze, M.; Köhler, W.; Wegner, G. submitted to *Macromolecules*.
(27) Hesse, M.; Meier, H.; Zeeh, B. *Spektroskopische Methoden in der organischen Chemie*; Georg Thieme Verlag: Stuttgart, 1984.
(28) Witteler, H. Ph.D. Thesis, University of Mainz, Mainz, Germany, 1993.
(29) McCarthy, T. F.; Witteler, H.; Pakula, T.; Wegner, G. *Macromolecules* **1995**, *28*, 8350.
(30) Vallee, A.; Besner, S.; Prud'Homme, J. *Electrochim. Acta* **1992**, *37*, 1579.
(31) Williams, M. L.; Landel, R. F.; Ferry, J. D. *J. Am. Chem. Soc.* **1955**, *77*, 3701.
(32) Ratner, M. A. In *Polymer Electrolyte Reviews*; MacCallum, J. R., Vincent, C. A., Eds.; Elsevier Applied Science: London 1987; Vol. 1.
(33) Watanabe, M.; Aoki, S.; Sanui, K.; Ogata, N. *Polym. Adv. Technol.* **1993**, *4*, 179.
(34) Benrabah, D.; Sanchez, J. Y.; Armand, M. *Solid State Ionics* **1993**, *60*, 87.
(35) Armand, M.; Gorecki, W.; Andreani, R. In *Second International Symposium on Polymer Electrolytes*; Scrosati, B., Ed.; Elsevier Applied Science: London, 1990.

MA961098Y